Hard X-ray phase imaging and tomography with a grating interferometer

Timm Weitkamp[a*], Ana Diaz[a], Bernd Nöhammer[a], Franz Pfeiffer[c], Torben Rohbeck[a], Peter Cloetens[b], Marco Stampanoni[c], and Christian David[a]

[a]Laboratory for Micro- And Nanotechnology, Paul Scherrer Institut, 5232 Villigen PSI, Switzerland

[b]European Synchrotron Radiation Facility, 6 rue Jules Horowitz, B. P. 220, 38043 Grenoble, France

[c]Swiss Light Source, Paul Scherrer Institut, 5232 Villigen PSI, Switzerland

ABSTRACT

We have developed a two-grating interferometer for hard X rays that can be used for phase imaging and tomography. A silicon phase grating positioned just downstream of the object under study splits the distorted wavefront into essentially a positive and a negative first-order beam. At a given distance from this beam-splitter grating, where the two beams still mostly overlap, they form a pattern of interference fringes that is distorted according to the wavefront distortions. The fringes may be finer than the resolution of an area detector used to record the signal, but an absorption grating with suitable pitch, put in front of the detection plane, allows the detection of intensity variations that correspond to the derivative of the wavefront phase taken along the direction perpendicular to the grating lines. A combination of this technique with the phase-stepping method, in which several exposures are made which differ in the phase of the fringe pattern, allows to eliminate effects of non-uniform intensity due to inhomogeneous illumination and edge-enhancing inline phase contrast. Several examples of tomograms taken under different experimental conditions are shown, including a polychromatic "pink-beam" setup.

Keywords: X-ray tomography, phase-stepping interferometry, synchrotron radiation, microtomography, phase reconstruction

1. INTRODUCTION

Phase-sensitive X-ray imaging techniques have seen intensive development in the past decade[1,2] because they have the potential of imaging weakly-absorbing structures such as soft biological tissue, polymers etc. with lower dose and higher contrast-to-noise ratio than conventional absorption radiography. The different methods proposed and demonstrated — commonly classified into interferometric methods,[3–6] techniques using an analyzer crystal[7,8] and free-space propagation methods[9–13] — differ vastly in the nature of the signal recorded, the experimental setup, and the requirements on the illuminating radiation (especially its spatial coherence and monochromaticity). Although some of these techniques yield excellent results for certain problems, none of them is as of today very widely used. In particular, none of them has so far found medical diagnostics applications, which require a large field of view of many centimeters, the efficient use of broadband radiation as provided by laboratory X-ray generators (rather than synchrotron radiation sources) and a reasonably compact setup. Here we present an interferometric X-ray phase imaging method in which some of the problems do not occur that so far impair the wider use of phase contrast in X-ray radiography and tomography.

2. PRINCIPLE

A transmission phase grating with periodicity g is placed in the X-ray beam. Downstream of the grating, the Talbot self-imaging effect then leads to linear periodic interference fringes in planes perpendicular to the optical axis. If the grating has a phase shift of π and the incident wave is plane, then these fringes have a periodicity of $g/2$, and their contrast is maximal at distances

$$D_n = n \times \frac{g^2}{8\lambda} \quad (n = 1, 3, 5, \ldots) \,. \tag{1}$$

*E-mail: timm.weitkamp@psi.ch; Telephone: +41 56 310 23 02; WWW: http://people.web.psi.ch/weitkamp/

For even values of n in the above equation, the contrast vanishes. In the case of a spherical or cylindrical incident wave with radius of curvature R instead of a plane wave, the fringe spacing is slightly different, and the Talbot distances are slightly shifted.

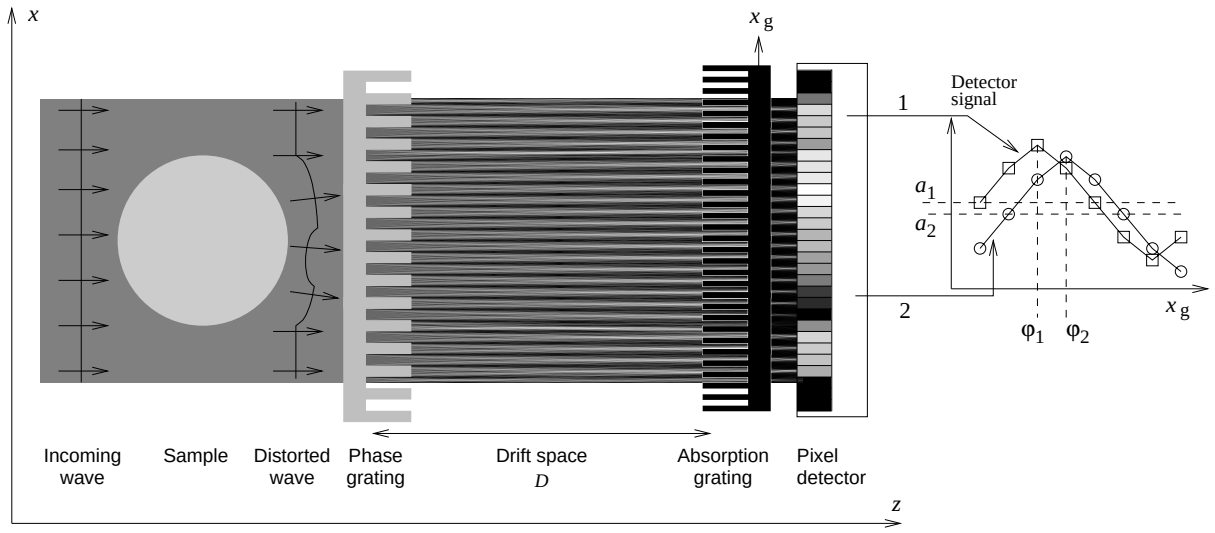

Figure 1: Principle of phase-contrast imaging with a grating interferometer. *Left to right:* the incoming X-ray wavefront is locally distorted by the sample. A phase grating placed in the beam leads to interference fringes. Where the wavefront is distorted, these fringes are displaced from their unperturbed position. The fringe displacements are transformed into intensity values by an absorption grating placed at a distance D from the phase grating. This allows the use of a detector with much larger pixels than the spacing of the fringes. Scanning the lateral position x_g of one of the gratings (here the absorption grating) causes the recorded signal in each pixel to oscillate as a function of x_g. The phase φ of the oscillation in each pixel is a measure of the wavefront phase gradient, while the average detector signal a in each pixel over the grating scan is equivalent to the non-interferometric image.

Perturbations of the incident wavefront, e. g., induced by an object in the beam, lead to a local displacement of the interference fringes (figure 1). The fringe displacement d observed at a distance D from the phase grating is

$$d = \frac{D\lambda}{2\pi} \frac{\partial \Phi}{\partial x} , \tag{2}$$

where λ is the radiation wavelength, Φ is the phase profile of the wavefront, and x is the transverse coordinate perpendicular to the grating lines.

The fundamental idea of the method presented here is to detect the positions of the fringes and determine from these the distortions of the wavefront.

In order for the fringes to be clearly visible, the projected source size at the observation position should not exceed a quarter of the fringe spacing. This corresponds to a required minimal transverse coherence length in the direction perpendicular to the grating lines of

$$\ell_{\mathrm{coh}} \geq ng \tag{3}$$

if the detection plane is located at one of the Talbot distances D_n from equation 1.

In order to keep the requirements on the coherence length ℓ_{coh} moderate, the periodicity g of the phase grating should not be larger than a few microns. Another reason for choosing a relatively small value of g is to keep the experimental setup compact (the Talbot distances D_n scale with the square of g, see equation 1).

With the periodicity g of the phase grating not exceeding a few microns and the periodicity of the phase fringes being close to $g/2$, an area detector placed in the detection plane will generally not have sufficient resolution to resolve the fringes, let alone resolve the position of the fringes with sub-fringewidth accuracy. Therefore, an absorption grating is placed into the beam in the detection plane. The periodicity of the absorption grating is chosen identical to the periodicity of the

unperturbed interference fringe pattern, ($g/2$ for a plane wave). Its lines are aligned parallel to the interference fringes. The absorption grating then acts as a transmission mask for the detector, which is placed directly behind it.

The absorption grating transforms fringe displacement into intensity variation. Assume first that the grating is placed so that the absorbing lines coincide with the intensity maxima of the unperturbed fringe pattern. Then the recorded intensity on the detector will be low because all the fringe intensity is absorbed in the opaque grating lines. However, in regions where the fringes are displaced, the recorded intensity will be higher because part of the fringe intensity passes through the grating. If now the grating is shifted transversely by a quarter of its period, then the recorded intensity in regions of unperturbed fringes will have an intermediate value. Fringes displaced in the direction towards the next opaque grating line will then result in lower intensity on the detector, while fringes displaced into the other direction will result in higher intensity. The use of the absorption grating as an analyzer makes the setup substantially simpler, more compact, and easier to use than a previous design with a second phase grating and analyzer crystal.[14]

If now the absorption grating is scanned along the transverse direction x over one entire period, then the intensity in each pixel (i, j) of the two-dimensional detector will oscillate as a function of grating position x_g. The phase of this oscillation, φ_{ij}, can be determined by analyzing the first Fourier component of the oscillation. It is obviously related to the displacement d_{ij} of the fringes at this position by

$$d_{ij} = \frac{\varphi_{ij}}{2\pi}\, g_2 \,, \tag{4}$$

where $g_2 \approx g/2$ is the period of the absorption grating. This method is known from other ranges of the electromagnetic spectrum as *phase-stepping interferometry*.[15] With equation 2, we obtain the first derivative of the wavefront phase profile in each pixel, $(\partial\Phi/\partial x)_{ij}$, as a function of intensity-oscillation phase φ_{ij}:

$$\left(\frac{\partial\Phi}{\partial x}\right)_{ij} = \frac{g_2}{\lambda D}\,\varphi_{ij} \,. \tag{5}$$

We note that the intensity-oscillation phase φ_{ij} contains no contributions from the amplitude profile of the wave. The phase profile Φ of the wavefront can be retrieved from φ by simple one-dimensional integration along the pixel direction perpendicular to the grating lines. For a plane incoming wave, Φ is the projection of the decrement of X-ray refractive index, δ, in the sample along the beam direction. A tomographic reconstruction of Φ therefore yields the three-dimensional distribution of δ in the sample. A flatfield correction that accounts for a non-plane incoming wave can easily be carried out by subtracting the phase profile of the beam without sample from the phase profile with the sample in the beam.

Another quantity that can be extracted from a phase-stepping scan is the radiograph that would be obtained without the interferometer in the beam. This is achieved by simple averaging the signal in each pixel over the points in one phase-stepping scan of the grating. The interferometric contrast then cancels out, leaving only the absorption and Fresnel inline contrast. This signal can be flatfield-corrected in the same way as in non-interferometric imaging, by division of an image obtained with the sample over an image without the sample.

An interferometer built and operated according to these principles thus offers the possibility of both phase and absorption/edge-enhanced radiography and tomographic imaging in a single scan.

An important property of this grating interferometer is that it is quasi-achromatic and can be used efficiently with broadband radiation. This is because the positions of the interference fringes downstream of the phase grating, as well as their displacement upon wavefront distortion, do not depend on photon energy. Under the conditions that the bandwidth of the radiation be small enough so that (1) the refractive index of the sample can be assumed to be constant over the energy bandwidth and (2) the Talbot distances do not change so much over the energy range that contrast reversal occurs, the instrument can therefore be operated with polychromatic radiation and still be used for quantitative phase imaging.

3. INSTRUMENTATION

The essential parts of an interferometer using the principles laid out above are the two gratings. Phase gratings were structured into 250-μm-thick silicon-111 chips by electron-beam lithography and subsequent KOH wet etching. Figure 2 (left) shows a phase grating obtained in this way. The structure height of the gratings is adapted to the design photon energy of the device so that the grating shifts the phase by exactly π. This ensures maximum efficiency of the grating by

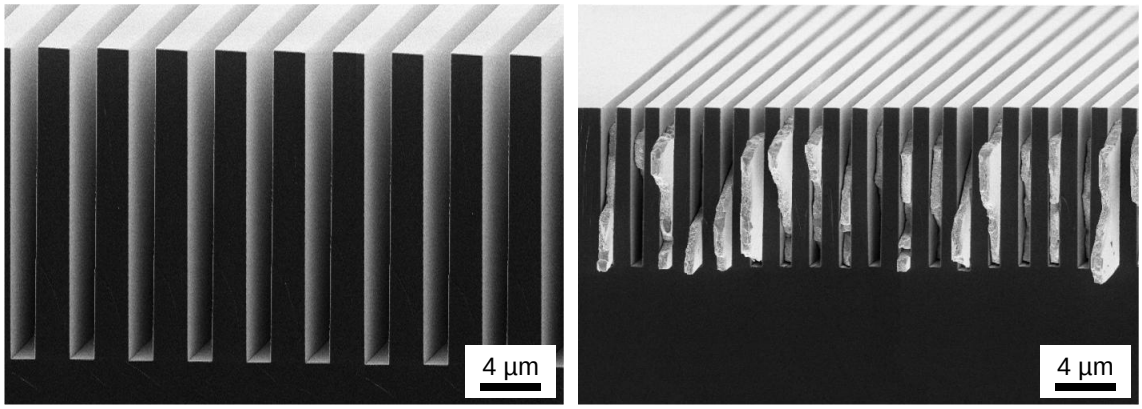

Figure 2: *Left:* Phase grating made of silicon, pitch $g = 4\ \mu\mathrm{m}$, structure height 21 $\mu\mathrm{m}$. *Right:* Gold absorption grating with a period of 2 $\mu\mathrm{m}$. The gold, grown electrochemically, can be seen in the gaps of the supporting silicon grating structure.

elimination of the zeroth diffraction order, or undiffracted part of the beam, although operation at other energies than the design energy is also possible.

The absorption gratings are made by electrochemical growth of gold into the gaps of a previously made silicon grating (figure 2, right).

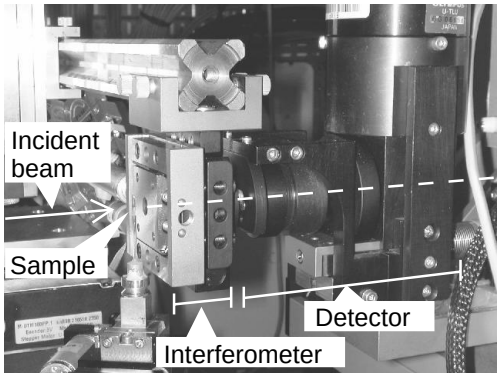

Figure 3: Picture of a typical interferometer setup (here mounted at the ESRF beamline ID 19). The beam enters from the left. The sample is mounted on a tomography sample stage (here with a vertical axis of rotation). The phase grating and the absorption grating of the interferometer are hidden, respectively, inside the translation stage placed downstream of the sample and between the interferometer and the objective holder of the camera.

The two gratings are then mounted on a stage with two motorized degrees of freedom: rotation of one of the gratings about the beam axis for alignment, and translation perpendicular to the grating lines for the other grating, for the phase-stepping scans. This whole stage can be made so compact that it can be fixed to the imaging detector, as shown in the picture in figure 3.

4. RESULTS

We used grating interferometers at different photon energies, radiation bandwidths, and Talbot distances for phase imaging and tomography. One of the first objects imaged in three dimensions with the device was a hair of one of the authors (A. D.) with a knot in it. Figure 4 shows projection images from a phase-stepping scan as well as a reconstructed phase tomogram and an isosurface rendering of the full volume dataset.

An example of a more complex object is shown in the left image of figure 5. The phase tomography of a spider in a field of view of (1.9 mm)^2 with a voxel size of 2 $\mu\mathrm{m}$ was taken at the ESRF beamline ID 19.

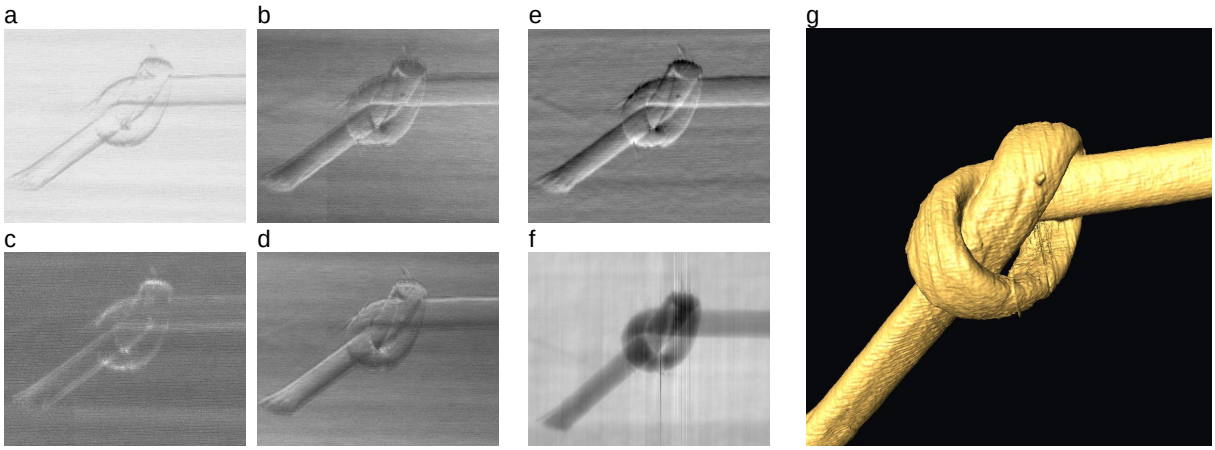

Figure 4: Phase-stepping tomography scan of a humain hair (diameter approx. 40 μm) with a knot. *a-d:* Raw interferograms taken at different lateral relative positions x_{g} of the gratings. *e:* Phase-gradient image φ. *f:* Reconstructed projected phase. *g:* Isosurface rendering of the reconstructed phase volume data. The experiment was carried out at the Materials Science beamline of the Swiss Light Source using monochromatic X rays of 14.4 keV energy. The gratings were positioned in the 3rd Talbot distance (79 mm), the phase grating period was $g = 4\ \mu\mathrm{m}$.

Tomographic datasets with broadband radiation were taken at the SLS Materials Science beamline. Here, the wiggler beam was conditioned by reflection on two mirror surfaces coated with rhodium at an incidence angle of 2.5 mrad to remove the high-energy part of the spectrum. It was then passed through a 100-μm-thick zirconium filter. The 20-μm-thick yttrium aluminum garnet (YAG) scintillator of the camera added a high-pass filter component. The resulting bandpass filter was centered around 17.5 keV with a bandwidth of almost exactly 1 keV. The panel on the right of figure 5 shows a three-dimensional rendering of a reference sample.

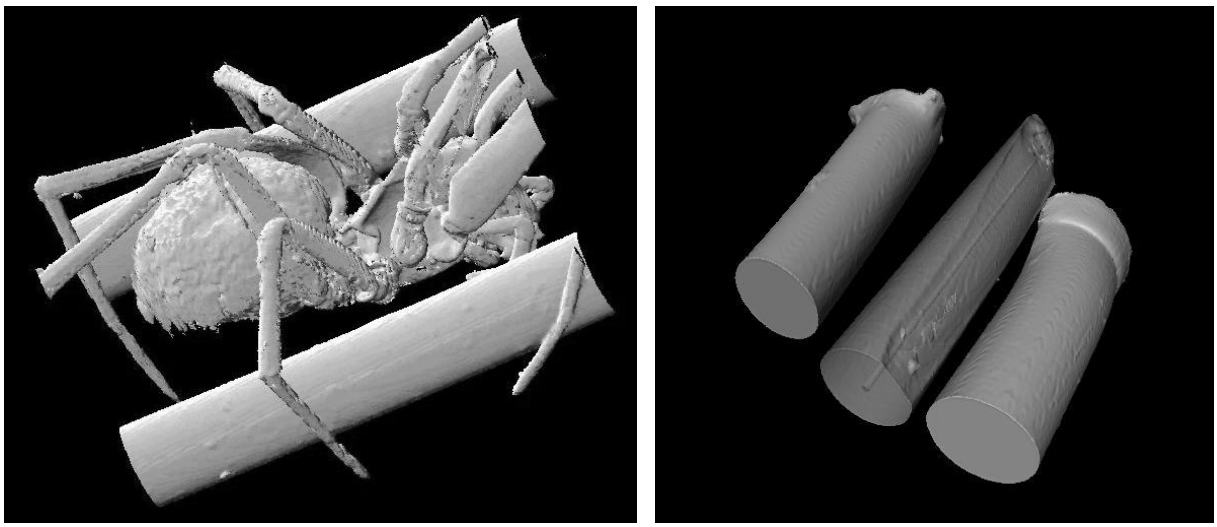

Figure 5: Isosurface renderings of reconstructed phase volume datasets taken under different conditions. *Left:* Small spider (reconstructed volume (1.9 mm)^3), taken at ESRF beamline ID 19, monochromatic 14.4-keV radiation, 1st Talbot distance (23 mm), phase grating period $g = 4\ \mu\mathrm{m}$. *Right:* Three fibers — the central one a 200-μm diameter boron fiber with a tungsten core, the outer ones made of different polymers — imaged with a pink beam of (17.5 ± 0.5) keV energy at the SLS Materials Science beamline.

5. CONCLUSIONS AND OUTLOOK

The instrument we have presented here is a compact and robust interferometer that can be used for phase imaging and tomography with monochromatic or broadband radiation. The requirements on beam coherence and mechanical stability are moderate, so that with an advanced setup operation on laboratory X-ray sources should be possible. The phase contribution to the signal can easily be separated from the absorption part, and the reconstruction of the phase from its first derivative along a fixed direction is much simpler than reconstruction techniques required for non-interferometric inline phase images. The lateral resolution of a projection image is limited by the shear of the two partial waves and amounts to a few microns. The field of view is currently 2 mm in both horizontal and vertical direction, but using photolithography techniques for grating production it can be extended without loss in resolution, given a sufficiently large detector.

REFERENCES

1. R. Fitzgerald, "Phase-sensitive x-ray imaging," *Physics Today* **53**, pp. 23–27, July 2000.
2. A. Momose, "Phase-sensitive imaging and phase tomography using X-ray interferometers," *Optics Express* **11**, pp. 2303–2314, 2003.
3. U. Bonse and M. Hart, "An X-ray interferometer," *Appl. Phys. Lett.* **6**, pp. 155–156, 1965.
4. A. Momose, T. Takeda, and Y. Itai, "Phase-contrast X-ray computed tomography for observing biological specimens and organic materials," *Rev. Sci. Instr.* **66**, pp. 1434–1436, 1995.
5. A. Momose, T. Takeda, Y. Itai, and K. Hirano, "Phase-contrast X-ray computed tomography for observing biological soft tissues," *Nature Med.* **2**, pp. 473–475, 1996.
6. F. Beckmann, U. Bonse, F. Busch, and O. Günnewig, "X-ray microtomography using phase contrast for the investigation of organic matter," *J. Comp. Assist. Tom.* **21**, pp. 539–553, 1997.
7. V. N. Ingal and E. A. Beliaevskaya, "X-ray plane-wave topography observation of the phase contrast from a non-crystalline object," *J. Phys. D* , 1995.
8. F. A. Dilmanian, Z. Zhong, B. Ren, X. Y. Wu, L. D. Chapman, I. Orion, and W. C. Thomlinson, "Computed tomography of x-ray index of refraction using the diffraction enhanced imaging method," *Phys. Med. Biol.* , 2000.
9. A. Snigirev, I. Snigireva, V. Kohn, S. Kuznetsov, and I. Schelokov, "On the possibilities of x-ray phase contrast microimaging by coherent high-energy synchrotron radiation," *Rev. Sci. Instr.* **66**, pp. 5486–5492, 1995.
10. P. Cloetens, R. Barrett, J. Baruchel, J.-P. Guigay, and M. Schlenker, "Phase objects in synchrotron radiation hard x-ray imaging," *J. Phys. D* **29**, pp. 133–146, 1996.
11. S. W. Wilkins, T. E. Gureyev, D. Gao, A. Pogany, and A. W. Stevenson, "Phase-contrast imaging using polychromatic hard x-rays," *Nature* **6607**, pp. 335–337, 1996.
12. P. Spanne, C. Raven, I. Snigireva, and A. Snigirev, "In-line holography and phase-contrast microtomography with high-energy X rays," *Phys. Med. Biol.* **44**, pp. 741–749, 1999.
13. P. Cloetens, W. Ludwig, J. Baruchel, D. V. Dyck, J. V. Landuyt, J. P. Guigay, and M. Schlenker, "Holotomography: Quantitative phase tomography with micrometer resolution using hard synchrotron radiation x rays," *Appl. Phys. Lett.* **75**, pp. 2912–2914, 1999.
14. C. David, B. Nöhammer, H. H. Solak, and E. Ziegler, "Differential x-ray phase contrast imaging using a shearing interferometer," *Appl. Phys. Lett.* **81**, pp. 3287–3289, 2002.
15. K. Creath, "Phase-measurement interferometry techniques," in *Progress In Optics XXVI*, E. Wolf, ed., pp. 349–393, Elsevier Science, 1988.